Journal Title: Nuclear science and engineering

Volume: 101
Issue: 4
Month/Year: April 1989
Pages: 341-51

Article Author: Lorence, Morel, Larsen

Article Title: An S_2 synthetic acceleration scheme for the one-dimensional S_n equations with linear discontinuous spatial differencing

Note:

NUCLEAR SCIENCE AND ENGINEERING: 101, 341-351 (1989)

An S_2 Synthetic Acceleration Scheme for the One-Dimensional S_n Equations with Linear Discontinuous Spatial Differencing

Leonard J. Lorence, Jr.

Sandia National Laboratories, Simulation Theory Division, 1231 Albuquerque, New Mexico 87115

J. E. Morel

Los Alamos National Laboratory, Applied Theoretical Physics Division Los Alamos, New Mexico 87545

and

Edward W. Larsen

The University of Michigan, Department of Nuclear Engineering Ann Arbor, Michigan 48109

Received July 8, 1988
Accepted November 28, 1988

Abstract—*An S_2 synthetic acceleration scheme is developed for the one-dimensional S_n equations (slab and sphere) with linear discontinuous spatial differencing. A Fourier analysis shows that the scheme is unconditionally stable for a model problem. Computational results demonstrate the effectiveness of the technique for varying cell thickness and scattering anisotropy.*

I. INTRODUCTION

Many diffusion synthetic acceleration (DSA) methods have been developed for accelerating the iterative convergence of S_n solutions. Early schemes were impractical because they became unstable with moderately thick spatial cells.[1] Alcouffe solved this problem by showing that stability can be achieved by deriving the spatially differenced diffusion equation used in the acceleration scheme directly from the differenced S_n equations. Using this approach, he derived an unconditionally stable DSA scheme for the diamond-differenced S_n equations.[2] However, a negative flux fixup algorithm is generally used in conjunction with spatial diamond differencing, and such algorithms can cause DSA to become unstable. This is not a serious problem in neutronics calculations because the spatial cell widths can generally be chosen such that negative flux fixups rarely occur.

To obtain better acceleration for charged-particle transport problems[3] with highly anisotropic scattering, Morel extended Alcouffe's method to accelerate both the zeroth and first moments of the scattering source.[4] The main result from this work is that two-moment DSA of the S_n equations with highly anisotropic scattering is significantly more effective than one-moment acceleration, but both schemes become increasingly susceptible to negative flux fixup destabilization with increasing scattering anisotropy. This implies that a reliable, efficient, and accurate S_n method for charged-particle calculations requires a two-moment acceleration method with a high-order spatial differencing scheme, such as the linear discontinuous (LD) scheme, which can generally be used without

fixup. Larsen[5] has developed such a scheme for the one-dimensional slab geometry equations, but generalization of this method to curvilinear one-dimensional geometries appears to be extremely difficult due to algebraic complexities associated with the derivation of a differenced diffusion equation from the differenced S_n equations.

The main objective of the present work is to avoid the algebraic complexities associated with deriving a differenced diffusion equation from the S_n equations by using the similarly differenced S_2 equations rather than the diffusion equation as the low-order operator in a synthetic acceleration scheme. This approach is currently limited to the one-dimensional S_n equations because there currently are no efficient techniques for solving the two-dimensional S_2 equations when the scattering ratio is close to unity. However, recent work by Larsen[6] indicates that our one-dimensional acceleration scheme could be generalized for two-dimensional calculations if an efficient technique for solving the two-dimensional S_2 equations were to become available.

The specific method that we have developed is a two-moment S_2 synthetic acceleration scheme for the general one-dimensional geometry S_n equations (slab and sphere) with LD spatial differencing. We have implemented this scheme in a new version of the ONETRAN code[7] that has additional improvements, including an angular differencing scheme that eliminates the flux dip[8] and a Galerkin quadrature[9] option. The purpose of this paper is to describe our acceleration scheme and present computational results that demonstrate its effectiveness for calculations with isotropic scattering and highly anisotropic scattering.

Our acceleration scheme is described in Sec. II. A Fourier analysis is performed for the scheme in Sec. III. Computational results are presented in Sec. IV, and conclusions are given in Sec. V.

II. THE S_2 SYNTHETIC ACCELERATION SCHEME

Neglecting spatial discretization, the two-moment DSA scheme for the one-group, one-dimensional slab geometry S_n equations can be expressed as follows[4]:

$$\mu_m \frac{d}{dx}\psi_m^{l+1/2} + \sigma_t \psi_m^{l+1/2} = \sum_{k=0}^{L} \frac{(2k+1)}{2}\sigma_k \phi_k^l P_k(\mu_m) + q_m \ , \quad m = 1,N \ , \tag{1}$$

$$\phi_k^{l+1/2} = \sum_{m=1}^{N} \psi_m^{l+1/2} P_k(\mu_m) w_m \ , \tag{1a}$$

$$R_k^{l+1/2} = \sigma_k(\phi_k^{l+1/2} - \phi_k^l) \ , \quad k = 0,1 \ , \tag{2}$$

$$\frac{-d}{dx}\left[D\frac{d}{dx}c_0^{l+1/2}\right] + \sigma_a c_0^{l+1/2} = R_0^{l+1/2} - 3\frac{d}{dx}[DR_1^{l+1/2}] \ , \tag{3a}$$

$$c_1^{l+1/2} = -D\frac{d}{dx}c_0^{l+1/2} + 3DR_1^{l+1/2} \ , \tag{3b}$$

$$\phi_k^{l+1} = \phi_k^{l+1/2} + c_k^{l+1/2} \ , \quad k = 0,1 \ , \tag{4a}$$

and

$$\phi_k^{l+1} = \phi_k^{l+1/2} \ , \quad k = 2,\ldots,L \ , \tag{4b}$$

where

μ_m = quadrature cosines

w_m = quadrature weights

ψ_m = discrete angular fluxes

ϕ_k = k'th Legendre moment of the angular flux

q_m = distributed angular source

σ_a = macroscopic absorption cross section

σ_t = macroscopic total cross section

σ_k = k'th Legendre moment of the scattering cross section

D = diffusion coefficient = $[3(\sigma_a + \sigma_0 - \sigma_1)]^{-1}$

$P_k(\mu)$ = Legendre polynomial of degree k

c_0 = accelerative correction for the scalar flux

c_1 = accelerative correction for the current

l = iteration index

L = degree of the cross-section expansion ($0 \le k \le L$)

N = order of the quadrature set ($1 \le m \le N$).

The basic idea of this scheme is straightforward. Equation (1) and (1a) correspond to the standard unaccelerated source iteration: One first solves the S_n equations using the previous iterate for the flux moments, and then calculates new flux moments using the latest iterate for the angular flux. If there were no acceleration, these two steps would constitute a complete iteration. Convergence acceleration is achieved by obtaining additive corrections for the first two flux moments by means of Eqs. (3a) and (3b). The motivation for Eqs. (3a) and (3b) follows from the fact that the exact correction for the angular flux iterate at step $l + \frac{1}{2}$, i.e.,

$$\epsilon_m^{l+1/2} = \psi_m - \psi_m^{l+1/2} \ , \tag{5}$$

where ψ_m denotes the exact S_n solution, satisfies

$$\mu_m \frac{d}{dx}\epsilon_m^{l+1/2} + \sigma_t \epsilon_m^{l+1/2} = \sum_{k=0}^{L} \frac{(2k+1)}{2} \sigma_k \xi_k^{l+1/2} P_k(\mu_m) + R_m^{l+1/2} , \quad m = 1, N , \tag{6}$$

where

$$\xi_k^{l+1/2} = \sum_{m=1}^{N} \epsilon_m^{l+1/2} P_k(\mu_m) w_m \tag{6a}$$

and

$$R_m^{l+1/2} = \sum_{k=0}^{L} \frac{(2k+1)}{2} \sigma_k (\phi_k^{l+1/2} - \phi_k^l) P_k(\mu_m) . \tag{6b}$$

Equations (3a) and (3b) are equivalent to a P_1 approximation to Eq. (6) (Ref. 4). To demonstrate this, we first make the standard P_1 approximation:

$$\epsilon_m^{l+1/2} = 0.5(c_0^{l+1/2} + 3c_1^{l+1/2}\mu_m) . \tag{7}$$

Then we substitute Eq. (7) into Eq. (6), and successively take the zeroth and first angular moments of Eq. (6) (using the S_n quadrature formula) to obtain the scalar balance equation,

$$\frac{\partial}{\partial x} c_1^{l+1/2} + \sigma_a c_0^{l+1/2} = \sigma_0(\phi_0^{l+1/2} - \phi_0^l) , \tag{8}$$

and the first-moment equation,

$$\frac{1}{3}\frac{\partial}{\partial x} c_0^{l+1/2} + (\sigma_a + \sigma_0 - \sigma_1) c_1^{l+1/2} = \sigma_1(\phi_1^{l+1/2} - \phi_1^l) , \tag{9}$$

respectively. Equation (3b) follows directly from Eq. (9), and Eq. (3a) is obtained by substituting Eq. (3b) into Eq. (8). Once c_0 and c_1 have been obtained, the iteration proceeds by calculating the corrected flux moments according to Eq. (4a), which follows directly from Eqs. (1a), (5), and (7). This completes the accelerated iteration. Equation (4b) simply expresses the fact that the higher order moments are not corrected, and thus are not "accelerated."

Because Eqs. (3a) and (3b) are equivalent to the P_1 approximation rather than to the standard diffusion approximation, this scheme is really a P_1 synthetic acceleration scheme. However, we refer to it as a two-moment DSA scheme to emphasize the fact that the P_1 equations are expressed in the form of a modified diffusion equation rather than in the standard P_1 form given by Eqs. (8) and (9). The diffusion form is sometimes preferred because it generally costs less to solve than the standard P_1 equations, but neglecting spatial differencing considerations, both forms are equivalent.

There is a third form for the P_1 equations that serves as the basis for our synthetic acceleration scheme. We refer to this set of equations as the P_1 equivalent S_2 equations. They are obtained by transforming Eqs. (8) and (9) from the moment basis (c_0, c_1) to the interpolatory basis (c^+, c^-), where

$$c_m = c^+(0.5)(1 + \sqrt{3}\mu_m) + c^-(0.5)(1 - \sqrt{3}\mu_m) . \tag{10}$$

From Eq. (10) one can see that c^+ and c^- represent the point values of the linear representation for $c(\mu)$ at $\mu = +1/\sqrt{3}$ and $-1/\sqrt{3}$, respectively. The relationships necessary to effect this transformation are as follows:

$$c_0 = c^+ + c^- , \tag{11a}$$

$$c_1 = (c^+ - c^-)/\sqrt{3} , \tag{11b}$$

$$c^+ = 0.5(c_0 + \sqrt{3}c_1) , \tag{11c}$$

and

$$c^- = 0.5(c_0 - \sqrt{3}c_1) , \tag{11d}$$

and the equations that result can be expressed as

$$\mu^+ \frac{\partial}{\partial x} c^+ + \sigma_t c^+ = \sum_{k=0}^{1} \frac{(2k+1)}{2} \sigma_k c_k P_k(\mu^+) + R^+ \tag{12a}$$

and

$$\mu^- \frac{\partial}{\partial x} c^- + \sigma_t c^- = \sum_{k=0}^{1} \frac{(2k+1)}{2} \sigma_k c_k P_k(\mu^-) + R^- , \tag{12b}$$

where

$$\mu^+ = \frac{1}{\sqrt{3}} , \quad \mu^- = -\frac{1}{\sqrt{3}} , \tag{12c}$$

$$R^+ = 0.5[\sigma_0(\phi_0^{l+1/2} - \phi_0^l) + 3\mu^+\sigma_1(\phi_1^{l+1/2} - \phi_1^l)] , \tag{12d}$$

and

$$R^- = 0.5[\sigma_0(\phi_0^{l+1/2} - \phi_0^l) + 3\mu^-\sigma_1(\phi_1^{l+1/2} - \phi_1^l)] . \tag{12e}$$

Equation (12a) and (12b) are in the form of the standard S_2 equations with Gaussian quadrature. However, the equations that result for spherical geometry differ from the standard Gauss S_2 equations in the treatment of the angular derivative term.[10] Specifically, the standard S_2 equations have an explicit treatment for this term that requires that the angular flux be calculated along a special "starting" direction, whereas the P_1 equivalent S_2 equations have an implicit treatment. Thus, the standard S_2 equations in curvilinear coordinates have three unknowns, but the P_1 equivalent S_2 equations have only two. The P_1 equivalent S_2 acceleration equations are given for slab

and spherical one-dimensional geometries in the Appendix.

Our acceleration scheme is obtained in two steps:

1. The P_1 equivalent S_2 equations are substituted for the P_1 equivalent diffusion equation in the standard two-moment algorithm. For the slab geometry case, this simply means that Eqs. (12a) and (12b) are substituted for Eqs. (3a) and (3b) and that Eqs. (11a) and (11b) are used to calculate c_0 and c_1 from c^+ and c^-.

2. Linear discontinuous spatial differencing is used for both the S_n and S_2 equations.

The LD spatially differenced S_n equations are given in a general one-dimensional geometry form in the ONETRAN manual.[7] When the S_2 acceleration equations are differenced, they generate a seven-diagonal coefficient matrix. These equations are more expensive to solve than the diffusion equation because the diffusion equation has only half the unknowns and generates a three-diagonal coefficient matrix. However, as shown later, the cost of directly solving the S_2 equation, is small compared to the cost of iteratively solving the S_n equations.

It is of interest to point out that the present scheme is closely related to Larsen's original scheme for the slab geometry case,[5] but it is not identical. Rather than using the differenced S_2 equations, the original method uses a P_1 equivalent diffusion equation derived directly from the differenced S_n equations being accelerated. This diffusion equation contains parameters that depend on the quadrature set used in the S_n equations. The original scheme becomes equivalent to the present scheme only if those parameters are calculated with the Gauss S_2 quadrature set. Thus, the two methods are rigorously equivalent only when the Gauss S_2 equations are being accelerated. However, the original scheme can be made identical to the present scheme (for the slab geometry case) by requiring that the diffusion equation parameters always be calculated with the Gauss S_2 quadrature set. Although this identification is possible in one-dimensional slab geometry, because no angular derivative terms are present, it does not hold in one-dimensional spherical or cylindrical geometries, where the original scheme has not been formulated.

We wish to emphasize that our acceleration method uses the P_1 equivalent S_2 equations, rather than the standard S_2 equations, to perform the "low-order" calculation. The P_1 equivalent and standard S_2 equations are identical in slab geometry, but are different in curvilinear geometries, due to a different treatment of the angular derivative term. In their analytical form, the P_1 equivalent S_2 equations are algebraically equivalent to the standard P_1 equations, but (in spherical and cylindrical geometries) the standard S_2 equations are not.

III. FOURIER ANALYSIS

In this section, we use Fourier analysis techniques to determine the stability and effectiveness of our S_2 acceleration scheme for an idealized class of problems. The details of our Fourier analysis differ from previously published analyses[5,11] in two respects: The LD spatial differencing scheme contains *two* unknowns per cell per direction (an "average" angular flux and a "slope" angular flux; these are defined below) and scattering is *arbitrarily anisotropic*. Nevertheless, our basic approach is similar to previous approaches, and our presentation here is, accordingly, brief.

In spatially analytic form, the S_2 acceleration method developed in Sec. II for slab geometry can be written as

$$\mu_m \frac{d}{dx}\psi_m^{l+1/2} + \sigma_t \psi_m^{l+1/2} = \sum_{k=0}^{L} \frac{(2k+1)}{2}\sigma_k \phi_k^l P_k(\mu_m) + q_m \ , \quad m = 1, N \ , \tag{13a}$$

$$\phi_k^{l+1/2} = \sum_{m=1}^{N} \psi_m^{l+1/2} P_k(\mu_m) w_m \ , \quad 0 \le k \le L \ , \tag{13b}$$

$$R^{\pm,l+1/2} = \frac{1}{2}\left[\sigma_0(\phi_0^{l+1/2} - \phi_0^l) \pm \sqrt{3}\sigma_1(\phi_1^{l+1/2} - \phi_1^l)\right] , \tag{13c}$$

$$\pm \frac{1}{\sqrt{3}}\frac{\partial}{\partial x} c^{\pm,l+1/2} + \sigma_t c^{\pm,l+1/2} = \frac{1}{2}\left[\sigma_0(c^{+,l+1/2} + c^{-,l+1/2}) \pm 3\sigma_1(c^{+,l+1/2} - c^{-,l+1/2})\right] + R^{\pm} \ , \tag{13d}$$

$$\phi_0^{l+1} = \phi_0^{l+1/2} + (c^{+,l+1/2} + c^{-,l+1/2}) \ , \tag{13e}$$

$$\phi_1^{l+1} = \phi_1^{l+1/2} + \frac{1}{\sqrt{3}}(c^{+,l+1/2} - c^{-,l+1/2}) \ , \tag{13f}$$

and

$$\phi_k^{l+1} = \phi_k^{l+1/2} \ , \quad 2 \le k \le L \ . \tag{13g}$$

To spatially discretize these equations, we use the same LD differencing scheme for the high-order S_n equations (13a) as for the low-order S_2 equations (13d). For the generic S_n equation

$$\mu_m \frac{d}{dx}\psi_m(x) + \sigma_t \psi_m(x) = S_m(x) \tag{14}$$

on the j'th spatial cell $x_{j-1/2} < x < x_{j+1/2}$, we now give a brief derivation of this method. Our analysis is algebraically equivalent to, but different in form from, previous derivations[7,10]; the approach here admits a simpler Fourier analysis.

To begin, we define the cell-average flux ψ_{mj} and the cell-average slope $\hat{\psi}_{mj}$ by

$$\psi_{mj} = \frac{1}{h_j} \int_{x_{j-1/2}}^{x_{j+1/2}} \psi_m(x)\, dx \tag{15a}$$

and

$$\hat{\psi}_{mj} = \frac{6}{h_j^2} \int_{x_{j-1/2}}^{x_{j+1/2}} (x - x_j)\psi_m(x)\, dx \ , \tag{15b}$$

where

$$h_j = x_{j+1/2} - x_{j-1/2}$$

and

$$x_j = (x_{j+1/2} + x_{j-1/2})/2 \ .$$

Then, if $\psi_m(x)$ is nearly a linear function of x across the cell, we have

$$\psi_m(x) \approx \psi_{mj} + \frac{2}{h_j} (x - x_j)\hat{\psi}_{mj}$$

and

$$x_{j-1/2} < x < x_{j+1/2} \ . \tag{15c}$$

Likewise, we define constants S_j and $\hat{S}_j$ in terms of the known source $S(x)$:

$$S_j = \frac{1}{h_j} \int_{x_{j-1/2}}^{x_{j+1/2}} S(x)\, dx \tag{16a}$$

and

$$\hat{S}_j = \frac{6}{h_j^2} \int_{x_{j-1/2}}^{x_{j+1/2}} (x - x_j)S(x)\, dx \ , \tag{16b}$$

and we have

$$S(x) \approx S_j + \frac{2}{h_j} (x - x_j)\hat{S}_{mj}$$

and

$$x_{j-1/2} < x < x_{j+1/2} \ . \tag{16c}$$

The LD discretization of Eq. (14) is now given by

$$\frac{\mu_m}{h_j} (\psi_{m,j+1/2} - \psi_{m,j-1/2}) + \sigma_t \psi_{mj} = S_j \ , \tag{17a}$$

$$3\frac{\mu_m}{h_j} (\psi_{m,j+1/2} + \psi_{m,j-1/2} - 2\psi_{mj}) + \sigma_t \hat{\psi}_{mj} = \hat{S}_j \ , \tag{17b}$$

and

$$\psi_{mj} \pm \hat{\psi}_{mj} = \psi_{m,j\pm1/2} \ , \quad \mu_m \gtrless 0 \ , \tag{17c}$$

where $\psi_{m,j\pm1/2} = \psi_m(x_{j\pm1/2})$. Equation (17a) is obtained by integrating Eq. (14) over the j'th cell and using Eqs. (15) and (16); Eq. (17b) is obtained by multiplying Eq. (14) by $(x - x_j)$, integrating over the j'th cell, and using Eqs. (15) and (16); Eq. (17c) is obtained by taking Eq. (15c) to hold at $x = x_{j\pm1/2}$ for $\mu \gtrless 0$. Equations (17) are three equations for the three unknowns ψ_{mj}, $\hat{\psi}_{mj}$, and the exiting flux ($\psi_{m,j+1/2}$ if $\mu_m > 0$, and $\psi_{m,j-1/2}$ if $\mu_m < 0$).

We apply this differencing scheme to solve Eqs. (13a) and (13d), and the right sides of these equations and the remaining Eqs. (13) are all written in a form that is consistent with Eq. (15c). For example, in Eq. (13a), we use

$$\phi_k^l(x) = \phi_{kj}^l + \frac{2}{h_j} (x - x_j)\hat{\phi}_{kj}^l \ , \tag{18a}$$

$$\phi_{kj}^l = \sum_{m=1}^{N} P_k(\mu_m)\psi_{mj}^l w_m \ , \tag{18b}$$

and

$$\hat{\phi}_{kj}^l = \sum_{m=1}^{N} P_k(\mu_m)\hat{\psi}_{mj}^l w_m \ . \tag{18c}$$

The Fourier analysis is now performed as follows. First, we subtract Eqs. (13) from the fully converged equations, that is, Eqs. (13) with no iteration superscripts, to obtain a system of equations for the "iteration errors" (e.g., $\psi_m^{l+1/2} - \psi_m$) between the various iterates and the converged solution. This system is of the form of Eqs. (13) with $q_m = 0$. Therefore, we henceforth regard $q_m = 0$ and interpret all of the remaining terms in Eq. (13) as iteration errors.

Second, we introduce a Fourier decomposition by assuming the spatial variation in all quantities to be of the form $\exp(i\sigma_t \lambda x)$. For example,

$$\phi_{kj}^l = \omega^l a_k \exp(i\sigma_t \lambda x_j) \ , \tag{19a}$$

$$\hat{\phi}_{kj}^l = \omega^l \hat{a}_k \exp(i\sigma_t \lambda x_j) \ , \tag{19b}$$

$$\psi_{mj}^{l+1/2} = \omega^l \alpha_m \exp(i\sigma_t \lambda x_j) \ , \tag{19c}$$

$$\hat{\psi}_{mj}^{l+1/2} = \omega^l \alpha_m \exp(i\sigma_t \lambda x_j) \ , \tag{19d}$$

and

$$\psi_{m,j+1/2}^{l+1/2} = \omega^l \beta_m \exp(i\sigma_t \lambda x_{j+1/2}) \ , \tag{19e}$$

etc.

Third, we introduce this ansatz into the discretized form of Eqs. (13) and, after much tedious algebra, reduce the resulting system of equations to a single matrix equation of the form

$$\omega \boldsymbol{A} = \mathbf{M} \cdot \boldsymbol{A} \ , \tag{20a}$$

where $\boldsymbol{A}$ is the $(L + 1) \times 1$ column vector

$$\boldsymbol{A}^T = (a_0, a_1, \ldots, a_L, \hat{a}_0, \hat{a}_1, \ldots, \hat{a}_L) \ , \tag{20b}$$

and the iteration matrix $\mathbf{M} = \mathbf{M}(\lambda)$ is a $(2L + 2) \times (2L + 2)$ matrix. We note that the components of the vector $\boldsymbol{A}$ are the coefficients of ϕ_{kj}^l and $\hat{\phi}_{kj}^l$ in Eqs. (19a) and (19b); these terms occur in the right side of Eq. (13a) and serve to "drive" the iteration scheme.

The explicit form of **M** is very complicated and is not of sufficient interest to warrant its lengthy derivation here. The main point is that for each λ, **M** has at most $2L + 2$ distinct eigenvalues, and the spectral radius ρ is defined as the largest (in modulus) of these eigenvalues, taken over $0 \leqq \lambda < \infty$:

$$\rho = \sup_{0 \leqq \lambda < \infty} \max_{\omega \in \sigma(\mathbf{M})} |\omega| \ . \tag{21}$$

It is clear from Eqs. (19) that ρ determines the overall rate of convergence (or divergence) of the method. Specifically, if $\rho < 1$, the method is stable, and the smaller the value of ρ, the more rapid the convergence. A value of $\rho < 1$ with $\rho \approx 1$ indicates a stable but slowly converging method.

We have calculated the eigenvalues of **M** for several cases. The first case corresponds to isotropic scattering with $\sigma_t = \sigma_0$, $\sigma_0 = 1$, $h = 1$, and Gauss S_8 quadrature. The eigenvalue moduli for the unaccelerated and accelerated iteration operators are plotted in Figs. 1 and 2, respectively. These plots show that the unaccelerated and accelerated spectral radii are unity and 0.2127, respectively. As expected, the accelerated spectral radius is essentially equivalent to that associated with DSA (Ref. 5). Although we do not give detailed results here, further calculations indicate that the scheme remains extremely effective regardless of quadrature order, scattering ratio, or cell thickness, provided that the scattering cross-section expansion is of degree <2.

A significant decrease in effectiveness can occur with scattering expansions of degree 2 or higher. This is to be expected, because only the zeroth and first angular flux moments are accelerated. Specifically, our Fourier analysis indicates that with higher order ($L > 1$) scattering expansions and $\sigma_t = \sigma_0$, the spectral radius lies between ρ_1 and ρ_2, where ρ_1 is the spectral radius calculated with all but the zeroth and first moments set to zero, and

$$\rho_2 = \max|\sigma_k/\sigma_0| \ , \quad k = 2, L \ . \tag{22}$$

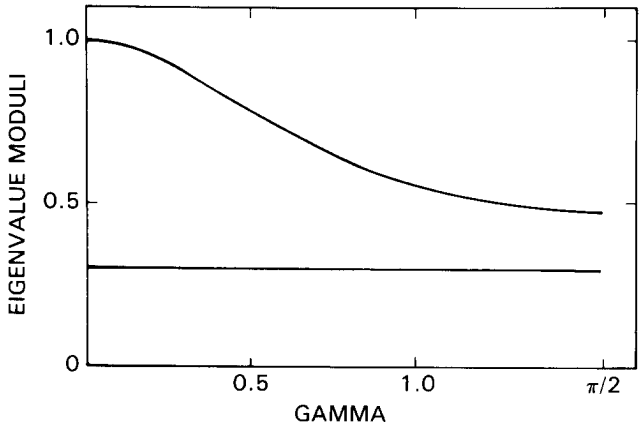

Fig. 1. Eigenvalue moduli for the isotropic scattering test case without acceleration.

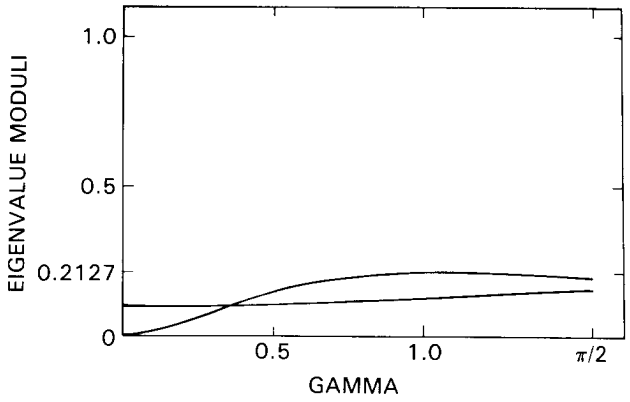

Fig. 2. Eigenvalue moduli for the isotropic scattering test case with acceleration.

Furthermore, if ρ_2 is sufficiently large, the spectral radius will be equal to ρ_2. With highly forward-peaked Fokker-Planck scattering,[3] the scattering coefficients are positive and monotonically decrease with k. Specifically,

$$\sigma_k = \sigma_0 - 0.5\sigma_{tr}k(k+1) \ , \quad k = 1, L \ , \tag{23a}$$

where

$$\sigma_0 = 0.5\sigma_{tr}L(L+1) \ , \tag{23b}$$

and σ_{tr} denotes the transport-corrected scattering cross section. The next expression follows from Eqs. (23):

$$\rho_2 = 1.0 - 6/[L(L+1)] \ . \tag{24}$$

Therefore, ρ_2 approaches unity in the limit as L increases without bound. Because the spectral radius is equal to ρ_2 if ρ_2 is sufficiently large, one finds that the spectral radius approaches unity in the same limit. Thus, with Fokker-Planck scattering, the accelerated spectral radius is always bounded away from unity, but it can be arbitrarily close to unity. The eigenvalue moduli for the unaccelerated and accelerated iteration matrices with P_7 Fokker-Planck scattering, S_8 Gauss quadrature, $\sigma_t = \sigma_0$, $\sigma_{tr} = 1$, and $h = 1$ are plotted in Figs. 3 and 4, respectively. Figure 4 shows an accelerated spectral radius of 0.8929, which agrees with that predicted by Eq. (24). We note that in Figs. 3 and 4, the largest (in magnitude) eigenvalue occurs at $\lambda = 0$, and that as λ increases, the largest (in magnitude) eigenvalue tends to monotonically decrease. Also, at $\lambda = 0$, all the eigenvalues ω are real, but as λ increases, most of these real eigenvalues coalesce into complex conjugate pairs.

IV. COMPUTATIONAL RESULTS

In this section, we present computational results that show that the S_2 acceleration scheme is effective for both isotropic and highly anisotropic scattering in

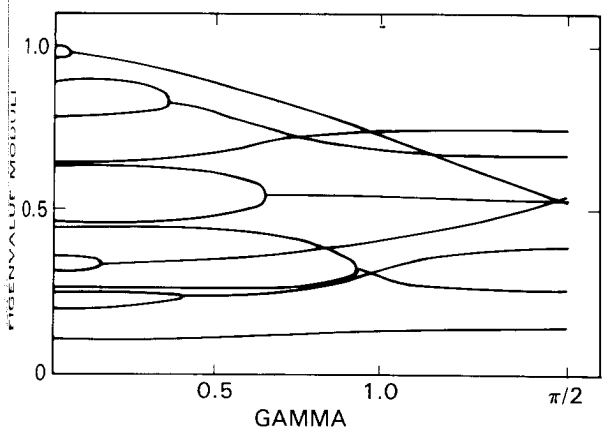

Fig. 3. Eigenvalue moduli for the anisotropic scattering test case without acceleration.

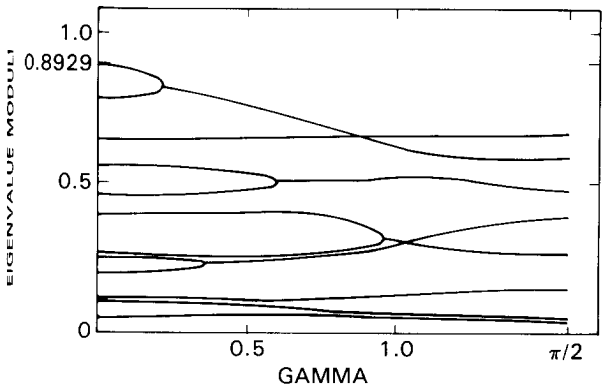

Fig. 4. Eigenvalue moduli for the anisotropic scattering test case with acceleration.

slab and spherical geometries. These results were obtained with a modified version of the ONETRAN code on the Cray XMP-48 at Sandia National Laboratories. In addition to accelerating the inner iterations with our new method, this version of ONETRAN uses the solution of the S_2 equations as the starting flux guess to begin the iterations.

Our first set of calculations pertain to P_1 scattering with varying degrees of anisotropy. The effectiveness of the S_2 acceleration scheme for slab and spherical geometries is shown in Tables I and II, respectively. Two other acceleration techniques (system rebalance and Chebyshev) that are presently available in ONETRAN are also included for comparison. In both the system rebalance and Chebyshev methods, only the zeroth Legendre moment of the flux is accelerated. While these schemes sometimes do not converge, the S_2 acceleration technique has never been observed to destabilize the inner iterations.

A nonabsorptive homogeneous medium was chosen for these problems together with a constant distributed isotropic source and vacuum boundary conditions. A Gauss S_4 quadrature was used for each discrete ordinates calculation. The slab width was selected to be 30 transport mean-free-paths, and 30 spatial mesh cells were used. Hence, the width of an individual mesh cell in total mean-free-paths $\sigma_t h$ increases as the average scattering cosine $\langle \mu \rangle$ increases.

As expected from the Fourier analysis of Sec. III, the S_2 scheme is uniformly effective for P_1 scattering, regardless of the severity of the anisotropy. In contrast, acceleration with either systemwide rebalance or Chebyshev becomes increasingly ineffective as the anisotropy is increased with P_1 scattering.

TABLE I

Slab Geometry P_1 Scattering and Isotropic Distributed Source

$\langle \mu \rangle$	$\sigma_t h$	Acceleration Technique	Iteration Count		ρ
			10^{-4}	$(1-\rho)10^{-4}$	
0	1.00	Rebalance	211	349	0.974
0	1.00	Chebyshev	93	126	0.924
0	1.00	S_2	5	6	0.13
0.25	1.33	Rebalance	264	458	0.980
0.25	1.33	Chebyshev	113	159	0.940
0.25	1.33	S_2	5	5	0.11
0.50	2.00	Rebalance	362	677	0.986
0.50	2.00	Chebyshev	174	270	0.965
0.50	2.00	S_2	5	5	0.101
0.75	4.00	Rebalance	616	1333	0.993
0.75	4.00	Chebyshev	274	465	0.980
0.75	4.00	S_2	5	5	0.08
0.95	20.00	Rebalance	1903	6579	0.999
0.95	20.00	S_2	5	5	0.135

TABLE II

Spherical Geometry P_1 Scattering and Isotropic Distributed Source

$\langle\mu\rangle$	$\sigma_t h$	Acceleration Technique	Iteration Count		ρ
			10^{-4}	$(1-\rho)10^{-4}$	
0	1.00	Rebalance	433	818	0.988
0	1.00	Chebyshev	178	269	0.964
0	1.00	S_2	5	6	0.137
0.25	1.33	Rebalance	542	1 083	0.991
0.25	1.33	Chebyshev	221	350	0.973
0.25	1.33	S_2	5	6	0.132
0.50	2.00	Rebalance	740	1 612	0.994
0.50	2.00	Chebyshev	350	619	0.985
0.50	2.00	S_2	5	5	0.101
0.75	4.00	Rebalance	1239	3 198	0.997
0.75	4.00	Chebyshev	552	1 091	0.991
0.75	4.00	S_2	5	5	0.076
0.95	20.00	Rebalance	3506	15 879	0.999
0.95	20.00	S_2	5	5	0.008

The iteration counts for two different convergence criteria are presented in Tables I and II. In the first, a relative pointwise convergence tolerance of 10^{-4} on the scalar flux was used. However, for acceleration with system rebalance and Chebyshev, this convergence test did not always guarantee an accurate computation of the scalar flux profile. For instance, the scalar flux profiles calculated with both S_2 and system rebalance acceleration in slab geometry for P_1 scattering ($\langle\mu\rangle = 0.95$) are shown in Fig. 5. At the middle of the slab, the two solutions differ by 7% when a relative convergence test of 10^{-4} is used. With a tighter convergence criterion, the scalar flux calculated with system rebalance acceleration agrees with that calculated with S_2 acceleration. Because a tighter convergence criterion does not appreciably change the scalar flux profile obtained from S_2 acceleration, the discrepancy shown in Fig. 5 is due to the false convergence of the inner iterations when system rebalance acceleration is used. Generally, false convergence is observed to be most significant when the spectral radius of the iteration process is very close to unity.

This can be seen from the following argument. (This brief analysis is well known in the numerical analysis community,[12] but not in the nuclear engineering community, so for completeness we present it here.) Suppose we have an iteration scheme

$$f^{l+1} = Lf^l + Q \ , \tag{25}$$

which stops iterating when

$$\|f^{l+1} - f^l\| < \delta \ . \tag{26}$$

Here, δ is a preassigned (small) number, termed the convergence criterion. Equation (25) implies

$$f^{l+1} = \sum_{k=0}^{l} L^k Q + L^{l+1} f^0 \ , \tag{27}$$

and letting f denote the exact solution of the problem, we have

$$f = \sum_{k=0}^{\infty} L^k Q \ . \tag{28}$$

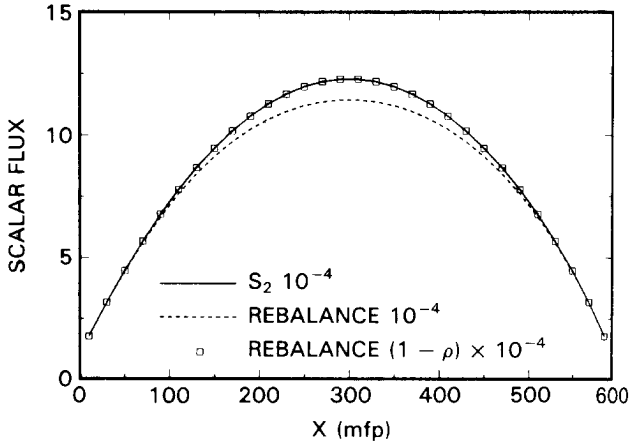

Fig. 5. Scalar flux spatial profile for P_1 scattering ($\langle\mu\rangle = 0.95$) with an isotropic distributed source in slab geometry.

Therefore,

$$f^{l+1} - f^l = L^l Q$$

and

$$f - f^{l+1} = \sum_{k=l+1}^{\infty} L^k Q - L^{l+1} f^0$$
$$= (I - L)^{-1} L^{l+1} Q - L^{l+1} f^0$$
$$= (I - L)^{-1} L (f^{l+1} - f^l) - L^{l+1} f^0 \quad . \quad (29)$$

This gives the rough estimate for large l:

$$\| f - f^{l+1} \| \sim \frac{1}{1 - \rho} \| f^{l+1} - f^l \| \quad , \quad (30)$$

where ρ is the spectral radius of L, assumed to be less than (but close to) unity. Thus, when the iterations cease, the actual error $\| f - f^{l+1} \|$ can be larger than the convergence criterion by the factor $(1 - \rho)^{-1}$, and to achieve an actual error of δ, the convergence criterion should be decreased by the factor $1 - \rho$.

It follows that the effectiveness of S_2 acceleration relative to rebalance and Chebyshev cannot be adequately guaged by comparing the iteration count for a relative convergence of 10^{-4}. To eliminate the possibility of false convergence, the tighter $(1 - \rho)10^{-4}$ relative convergence criterion on the scalar flux should be used, and these results are also shown in the tables. Our experience with this criterion indicates that it does in fact achieve 10^{-4} accuracy. The spectral radius is estimated on each iteration l in the following fashion:

$$\rho = \frac{\| \epsilon^l \|}{\| \epsilon^{l-1} \|} \quad ,$$

where

$$\| \epsilon^l \| = \left[\sum_i (\phi_i^l - \phi_i^{l-1})^2 \right]^{1/2} \quad . \quad (31)$$

The summation in Eq. (31) extends over all spatial points and ϕ is the scalar flux.

With this tighter convergence criterion, the efficiency of S_2 acceleration increases relative to both system rebalance and Chebyshev. As shown in Fig. 5, the tighter convergence criterion is necessary if the false convergence of solutions obtained with system rebalance acceleration is to be avoided.

The next set of calculations shown in Tables III

TABLE III

Slab Geometry Fokker-Planck Scattering and Isotropic Distributed Source

$\langle \mu \rangle$	$\sigma_t h$	Legendre Order	Scheme	Iteration Count 10^{-4}	Iteration Count $(1 - \rho)10^{-4}$	ρ
0.8333	2.00	3	Rebalance	152	234	0.96
0.8333	2.00	3	S_2	9	10	0.485
0.9643	9.33	7	Rebalance	512	1036	0.991
0.9643	9.33	7	S_2	25	43	0.890
0.9917	40.00	15	Rebalance	1490	4390	0.998
0.9917	40.00	15	S_2	70	182	0.974

TABLE IV

Spherical Geometry Fokker-Planck Scattering and Isotropic Distributed Source

$\langle \mu \rangle$	$\sigma_t h$	Legendre Order	Scheme	Iteration Count 10^{-4}	Iteration Count $(1 - \rho)10^{-4}$	ρ
0.8333	2.00	3	Rebalance	316	552	0.983
0.8333	2.00	3	S_2	9	9	0.380
0.9643	9.33	7	Rebalance	1044	2529	0.996
0.9643	9.33	7	S_2	27	42	0.874
0.9917	40.00	15	Rebalance	2841	10786	0.999
0.9917	40.00	15	S_2	77	178	0.971

and IV pertains to Fokker-Planck scattering.[3] For these problems, the medium is nonabsorptive and homogeneous. A constant distributed isotropic source and vacuum boundary conditions were also used. The width of medium was selected to be 10 transport mean-free-paths. In slab and spherical geometries, discrete ordinates calculations with Fokker-Planck scattering require that a Gauss quadrature set of order N be used in conjunction with Legendre expansions of order $N-1$.

In addition to being highly anisotropic, the Fokker-Planck scattering cross sections are represented by expansions of higher Legendre order. As expected from the analysis of Sec. III, the effectiveness of the S_2 acceleration scheme decreases as the Legendre order of the expansion increases. However, the S_2 method is always much more effective than either system rebalance or Chebyshev.

The S_2 acceleration technique does increase the cost of an inner iteration because the direct solution of Eqs. (12) must be obtained in each iteration. For the Fokker-Planck computations, the S_2 acceleration increases the cost of an iteration by 50% for an S_4 inner iteration and by 7% for an S_{16} inner iteration. Because S_2 acceleration substantially reduces the iteration count for these problems, the computational cost of performing the inner iterations is much less when S_2 acceleration is used than when either system rebalance or Chebyshev is employed.

V. CONCLUSIONS

We have shown that the P_1 equivalent S_2 synthetic acceleration scheme is an effective way of accelerating the one-dimensional S_n equations with LD spatial differencing. A Fourier analysis for a model problem indicates that this technique is uniformly effective for P_1 anisotropic scattering, and computational results in slab and spherical geometries indicate that this conclusion is valid for realistic problems. For higher order anisotropic scattering, such as Fokker-Planck scattering, a Fourier analysis and numerical experimentation show that S_2 synthetic acceleration is still much more effective than either system rebalance or Chebyshev acceleration. However, the efficiency of a two-moment acceleration scheme such as the S_2 method does degrade as the Legendre order of the scattering increases.

APPENDIX

The P_1 Equivalent S_2 Acceleration Equations

All quantities appearing in the following equations that are not explicitly defined in this Appendix are defined in the text. The P_1 equivalent S_2 acceleration equations follow.

Slab geometry:

$$\mu^+ \frac{dc^+}{dz} + \sigma_t c^+ = \frac{(\sigma_0+\sigma_1)c^+}{2} + \frac{(\sigma_0-\sigma_1)c^-}{2} + R^+ \tag{A.1}$$

and

$$\mu^- \frac{dc^-}{dz} + \sigma_t c^- = \frac{(\sigma_0-\sigma_1)c^+}{2} + \frac{(\sigma_0+\sigma_1)c^-}{2} + R^- . \tag{A.2}$$

Spherical geometry:

$$\frac{\mu^+}{r^2}\frac{d}{dr}(r^2c^+) - \frac{\mu^+}{r}(c^+ + c^-) + \sigma_t c^+ = \frac{(\sigma_0+\sigma_1)c^+}{2} + \frac{(\sigma_0-\sigma_1)c^-}{2} + R^+ \tag{A.3}$$

and

$$\frac{\mu^-}{r^2}\frac{d}{dr}(r^2c^-) - \frac{\mu^-}{r}(c^+ + c^-) + \sigma_t c^- = \frac{(\sigma_0-\sigma_1)c^+}{2} + \frac{(\sigma_0+\sigma_1)c^-}{2} + R^- . \tag{A.4}$$

Standard boundary conditions for the acceleration equations follow.

Left vacuum boundary condition:

$$c^+ = c^- \frac{(\mu^+ - \langle\mu\rangle)}{(\mu^+ + \langle\mu\rangle)} , \tag{A.5}$$

where

$$\langle\mu\rangle = W_s^{-1} \sum_{m=1}^{N} |\mu_m| w_m \tag{A.6}$$

and

$$W_s = \sum_{m=1}^{N} w_m . \tag{A.7}$$

Right vacuum boundary condition:

$$c^- = c^+ \frac{(\mu^+ - \langle\mu\rangle)}{(\mu^+ + \langle\mu\rangle)} . \tag{A.8}$$

Left reflective boundary condition:

$$c^+ = c^- - \frac{2}{W_s\mu^+} \sum_{m=1}^{N} \psi_m^{l+1/2} \mu_m w_m . \tag{A.9}$$

Right reflective boundary condition:

$$c^- = c^+ + \frac{2}{W_s\mu^+} \sum_{m=1}^{N} \psi_m^{l+1/2} \mu_m w_m . \tag{A.10}$$

Left periodic boundary condition:

$$c_L^+ = c_R^+ + (c_L^- - c_R^-)\frac{(\mu^+ - \langle\mu\rangle)}{(\mu^+ + \langle\mu\rangle)} + \frac{2}{W_s(\mu^+ + \langle\mu\rangle)}\sum_{\mu_m>0}(\psi_{R,m}^{l+1/2} - \psi_{L,m}^{l+1/2})\mu_m w_m , \quad (A.11)$$

where the subscripts L and R denote quantities located at the left and right boundaries, respectively.

Right periodic boundary condition:

$$c_R^- = c_L^- + (c_R^+ - c_L^+)\frac{(\mu^+ - \langle\mu\rangle)}{(\mu^+ + \langle\mu\rangle)} + \frac{2}{W_s(\mu^+ + \langle\mu\rangle)}\sum_{\mu_m<0}(\psi_{L,m}^{l+1/2} - \psi_{R,m}^{l+1/2})\mu_m w_m . \quad (A.12)$$

All of the preceding equations are derived by requiring that the accelerated iterate satisfy the exact boundary condition in an integral sense. For instance, at a left vacuum boundary, the accelerated iterate satisfies

$$\psi_m^{l+1} = 0 , \quad \mu_m > 0 . \quad (A.13)$$

The accelerated iterate is the sum of the iterate after the transport sweep and the S_2 correction to this iterate:

$$\psi_m^{l+1} = \psi_m^{l+1/2} + \frac{c_0^{l+1}}{2} + \frac{3}{2}c_1^{l+1}\mu_m . \quad (A.14)$$

Since Eq. (A.13) generally cannot be satisfied by the accelerated iterate, we require that the first half-range moment of that equation be satisfied:

$$\sum_{\mu_m>0}\left(\psi_m^{l+1/2} + \frac{c_0^{l+1}}{2} + \frac{3c_1^{l+1}}{2}\mu_m\right)\mu_m w_m = 0 . \quad (A.15)$$

Recognizing that $\psi_m^{l+1/2} = 0$ for $\mu_m > 0$, evaluating the sums, and transforming from the (c_0, c_1) representation in Eq. (A.15) to the (c^+, c^-) representation using Eqs. (11a) and (11b), we obtain Eq. (A.5).

All of the equations in this Appendix, with the exception of Eqs. (A.14) and (A.15), apply with an arbitrary normalization of the quadrature weights under the assumption that the same normalization is used in both the S_n equations and the S_2 acceleration equations. For simplicity, the equations in the text were derived under the assumption that the quadrature weights sum to two. The only effect of the quadrature normalization on the S_n equations is to scale the scattering source:

$$S_m = W_s^{-1}\sum_{k=0}^{L}(2k+1)\phi_k P_k(\mu_m) . \quad (A.16)$$

Thus, in accordance with Eqs. (A.16), (12d), and (12e), the residuals appearing in Eqs. (A.1) and (A.2) take the following form with arbitrary quadrature normalization:

$$R^+ = W_s^{-1}[\sigma_0(\phi_0^{l+1/2} - \phi_0^l) + 3\mu^+\sigma_1(\phi_1^{l+1/2} - \phi_1^l)] \quad (A.17)$$

and

$$R^- = W_s^{-1}[\sigma_0(\phi_0^{l+1/2} - \phi_0^l) + 3\mu^-\sigma_1(\phi_1^{l+1/2} - \phi_1^l)] . \quad (A.18)$$

ACKNOWLEDGMENT

This work was supported by the U.S. Department of Energy under contract DE-AC04-76DP00789.

REFERENCES

1. W. H. REED, *Nucl. Sci. Eng.*, **45**, 245 (1971).

2. R. E. ALCOUFFE, *Nucl. Sci. Eng.*, **64**, 344 (1977).

3. J. E. MOREL, *Nucl. Sci. Eng.*, **79**, 340 (1981).

4. J. E. MOREL, *Nucl. Sci. Eng.*, **82**, 34 (1982).

5. E. W. LARSEN, *Nucl. Sci. Eng.*, **82**, 47 (1982).

6. R. D. O'DELL, "Radiation Transport, April 1, 1986–December 31, 1986," Progress Report LA-10189-PR, Los Alamos National Laboratory (Oct. 1984).

7. T. R. HILL, "ONETRAN: A Discrete Ordinates Finite Element Code for the Solution of the One-Dimensional Multigroup Transport Equation," LA-5990-MS, Los Alamos National Laboratory (1973).

8. J. E. MOREL and G. R. MONTRY, *Transp. Theory Stat. Phys.*, **13**, 615 (1984).

9. J. E. MOREL, *Trans. Am. Nucl. Soc.*, **39**, 459 (1981).

10. E. E. LEWIS and W. F. MILLER, Jr., *Computational Methods of Neutron Transport*, Wiley, New York (1984).

11. D. VALOUGEORGIS, M. WILLIAMS, and E. W. LARSEN, *Nucl. Sci. Eng.*, **99**, 91 (1988).

12. L. A. HAGEMAN and D. M. YOUNG, *Applied Iterative Methods*, Academic Press, Inc., New York (1981).